Proceedings of the 8th North American International Conference on Industrial Engineering and Operations Management, Houston, Texas, USA, June 13-16, 2023

Design of MR Damper for Automobile Suspension with Finite Element Method

Aamar Shabir
Department of Electrical and Computer Engineering
Florida Polytechnic University
Lakeland, Florida, USA
ashabir0194@floridapoly.edu

Umar Irshad, Muhammad Shoaib and Huzaifa Abeer
Department of Electrical and Computer Engineering
NFC Institute of Engineering and Technology
Multan, Pakistan
umarirshad266@gmail.com, shoaibele120@gmail.com, theorientive1995@gmail.com

Abstract

In this paper, a new energy generated semi-active suspension system based on Magneto-rheological (MR) damper has been designed with the investigation of its power generation capability. The mathematical model for the suggested energy generated MR damper has developed and a 3D model of energy generated MR damper has developed in EMS, where it is analyzed broadly by finite element method. The objectives of the simulation were to minimize the interaction issue between the damper and energy generator parts and confirm its power generation ability. The induced magnetic flux density, magnetic field intensity, applied current density, temperature gradient of this damper clearly validated this damper's power generation.

Keywords

MR damper, EMS, Energy generation, vehicle suspension.

1. Introduction

MR fluid-based dampers so hopeful for semi-active or adaptive control system which's filled with kind of smart materials like Magneto rheological (MR) fluids (Lai et al 2002). MR fluid is made by mixing fine particles of carbonyl iron with low viscosity oil. It functions at three different mode such as shear mode, squeeze mode and valve mode. In the presence of an external magnetic or electric field MR fluids offer quick, reversible, and harmonic exchange to semi-solid state from free-flowing state in a few milliseconds and able to form chain-like fibrous structure . It has some striking benefits such as exhibiting a much lower sedimentation rate than conventional fluids, and a large operational temperature range . Moreover, it glances an improvement in apparent yield stress , quick response, and low power consumption . MR dampers is vast for both low- and high-speed (Shakil et al 2023). It's mainly used in automobiles, civil construction such as buildings, bridge's structure (Shabir et al 2022), reducing floor vibrations (Shabir et al 2022), heavy motor damping (Lai et al 2002), helicopter lag dampers(Shabir et al 2022), railway vehicles (Shabir et al 2022) and more (Shabir et al 2023). MR damper consists of a piston rod, a piston head, hydraulic and pneumatic reservoirs. These hydraulic and pneumatic reservoirs are separated by a floating piston or diaphragm (Shakil et al 2022). The piston head is attached by piston rod, and it contains magnetic circuit (coil on bobbin concentric to a tubular flux return). When the piston rod assembly moves inside the MR damper, the fluid flows by a circular gap in the piston head and creates a magnetic field in the gap and raises the yield stress of the MR fluid in the circular gap when current supplied to the coil in the piston head. Figure 1 shows the schematic diagram of the conventional semi-active suspension system. MR damper's vibration and shock create mechanical energy which can be used as a power sources and huge amount of this mechanical energy is lost during everyday usage of an automobile under road irregularities. By that the wasted energy vibration is attached with highway roughness, car speed, suspension rigid and damping coefficient and one report says that the total power dissipation of four dampers of traveler vehicle reached 200 W when going on a haggard highway at more or less 13.4 (Shabir et al 2022). External

power supply would not be needed, if this wasted energy can be transferred into the electrical energy (Shabir et al 2022). Suda et al observed that producing energy in the reproduction process is well to fulfill the energy demand in the dampers (Shabir et al 2022). Some research has been accomplished formerly on power generation ability of MR damper such as Jung et al introduced an MR damper with power regeneration which consists of an electromagnetic induction device for reducing suspension vibrations (Shabir et al 2022). It gives a technological plan for self-powered vibration control and electromagnetic induction (EMI) exploits vibration energy to produce electrical energy. Choi and Werely studied the liability and effectiveness of a self-powered MR damper and used a spring–mass electromagnetic induction device (Shabir et al 2022). The produced energy is used as the source of MR damper outright to escape the use of accessory sensors in the former two works. Bogdan et al introduced a power generator for a linear MR damper which is known as electromagnetic power generator (Shabir et al 2022). Chan et al first proposed the concept of self-powered, self-sensing MR dampers and filed for patent applications (Madiha et al 2023). It's only applicable for double ended MR dampers. With the aim of reducing the used amount of electric power increase reliability of the MR damper, this paper is proposing a new design concept for the magnetizing device involving a hybridized magnetic field source using a permanent magnet and coil concept for energy generation ability. It would be useful to incorporate the energy creation and manageable damping technological innovation within one system (Shakil et al 2022).

1.1 Objectives

This research focused on the Design of MR Damper for Automobile suspension with Finite Element method

2. Design Description of the Suggested Energy Generated MR Damper

The MR damper has two parts, one is damper parts and another is energy generation parts. The damping parts like a conventional damper but the energy generation parts consist a permanent magnet and coil arrangement. Figure 1 (a) presents a conventional MR damper and Figure 1 (b) displays the suggested mono tube MR damper. The proposed energy generated MR damper consists an extra permanent magnet, The nonmagnetic material is attached to the outside wall of the damper and permanent magnet is attached to nonmagnetic material. The external coil is attached to piston road. When the piston moves, the external coil moves with piston rod and cuts magnetic flux produced by the permanent magnet and produces electrical power (Shabir et al 2022).

From the cross section view of the Model damper, the position of the coil and permanent magnet is clearly observed. There's a small air gap between to the coils and a permanent magnet by which the permanent magnets move from

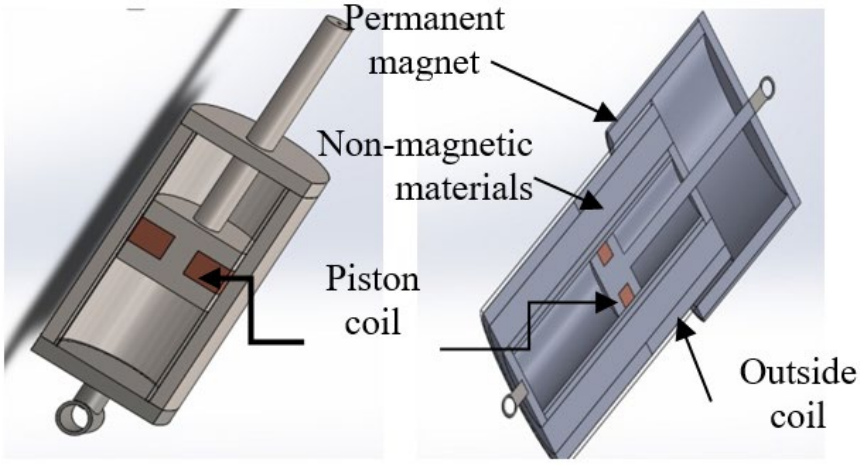

Figure1: (a) MR damper, (b) Suggested MR damper model

up to down during the piston's movement (Shabir et al 2022).

3. Mathematical Model of the Proposed Energy Generated MR Damper

The vibrations can be created power in the form of kinetic power. The technical power from the moving damper can be transformed into power which MR damper device can use it. The electro-magnetic transduction procedure is used here to quintessence power. The permanent magnets are made of neodymium magnet (NdFeB) grade N6 and non-magnetic materials are made of non-magnetic aluminum (lui et al 2022). Table 1 summarized below.

Table1: Specification of power generator

Parameter	Value
Magnet thickness τ_m	8 mm
Magnet quantity n_m	6
Gap distance g	3 mm
Coil turns N	250
Coil thickness w_c	6 mm
Magnet height l_m	46 mm
Resistance of the coil R_{coil}	2.6 Ω
Copper wire diameter	0.6 mm

According to the simulation, the height of the permanent magnet is taken 46 mm and the height as coil is selected 55 mm winding. The air gap magnetic flux is expressed by Equation (1) [32].

$$\Phi_g = \frac{B_{rem}\tau_m\mu_0 H_c A_g}{2gB_{rem} + \tau_m\mu_0 H_c \frac{A_g}{A_m}} \qquad (1)$$

Here Φ_g is the air gap magnetic flux without considering the flow, $\mu_0 = 4\pi \times 10^{-7}(NA^{-2})$, H_c is the coercive magnetic- field intensity of the magnet. Likewise, B_{rem} is the remanent flux density of the magnet, $A_g$is the area of the air gap and A_m is the area of the magnet. $\emptyset_g$ is the air-gap magnetic flux considering the flow.

$$\emptyset_g = \eta_1 \frac{B_{rem}\tau_m\mu_0 H_c A_g}{2gB_{rem} + \tau_m\mu_0 H_c \frac{A_g}{A_m}} \qquad (2)$$

In the event that the piston rod is permitted to move, then the magnet will move along the coil axis, an electric field will grow in the coil, for example, to restrict the magnet's movement. This field creates an electric potential V over the coil's leads, which Faraday's law of incitement predicts to be relative to the time rate of modifying in magnetic flux through the coil (Shakil et al 2022). Avoiding eddy current problems, the induced voltage can be mentioned as Equation 3.

$$V = -\frac{d}{dt}\oint_S^0 B.da = -\dot{\Phi}_{tot} \qquad (3)$$

A. The Force applied between the cylindrical permanent magnets and the coils of the MR damper

An analytical model is present in this study for calculating the applied axial force among the coils and cyliderical permanent magnets. The analyitical evolution of the axial force is stated by this Equation 4.

$$F_z = \frac{\mu_0 \kappa_1 \kappa_2}{4\pi} \iint_{S_1}^{0} \iint_{S_2}^{0} \frac{(\tilde{\tilde{z}} - \tilde{z}) \cos(\tilde{\theta}) \tilde{r} \tilde{\tilde{r}} d\tilde{\theta} d\tilde{z} d\tilde{\tilde{\theta}} d\tilde{\tilde{z}}}{(\tilde{\tilde{r}}^2 + \tilde{r}^2 - 2\tilde{r}\tilde{\tilde{r}} \cos(\tilde{\theta}) + (\tilde{\tilde{z}} - \tilde{z})^2)^{\frac{3}{2}}} \quad (4)$$

After assimilating $\tilde{z}, \tilde{\tilde{z}}, \tilde{\theta}$ *and* $\tilde{\tilde{\theta}}$ the applied force F_z between the permanent magnet and coils is stated finaly by Equation 5.

$$F_z = \frac{\mu_0 \kappa_1 \kappa_2}{2} C_d \quad (5)$$

$$C_d = \sum_{i=1}^{2} \sum_{j=3}^{4} (-1)^{i+j} (r_1 r_2)(A_z + f_z) \quad (6)$$

In Equation 7 A_z is absolutely analytical part and f_z is analytical part based on elliptic meanings.

$$A_z = \frac{(\varpi^2 - \tau)\pi - 2\sqrt{\nu}}{2\epsilon} \ln\left[\frac{-4\epsilon^2}{\nu^{\frac{3}{2}}}\right] - \frac{(\tau - \varpi^2)\pi - 2\sqrt{\nu}}{2\epsilon} \ln\left[\frac{4\epsilon^2}{\nu^{\frac{3}{2}}}\right] \quad (7)$$

$$f_z = \frac{2\mathbb{i}\varpi}{\epsilon\sqrt{\tau + \epsilon}} \left\{ (\tau + \epsilon) E\left[arc \sin \sqrt{\frac{1}{\psi}}, \psi \right] - \epsilon F\left[arc \sin \sqrt{\frac{1}{\psi}}, \psi \right] \right\}$$
$$+ \frac{2\varpi}{\kappa\sqrt{\beta}} \left\{ \frac{\epsilon}{\iota} E[\psi] - \epsilon\sqrt{\iota} K[\psi] + \sqrt{\beta\psi} \left((\tau - \varpi^2) K[2\iota] + \gamma \Pi[2\delta, 2\iota] \right) \right\} \quad (8)$$

The different parameters depend on i and j and the parameter i verifies $i^2 = -1$. The cylindrical permanent magnet is axially magnetized and the axial force applied between the cylindrical permanent magnets and coil is expressed directly by using the Equation 9.

$$F_z = \frac{J_1 J_2}{2\mu_0} C_d \quad (9)$$

B. Damping Force of the Proposed MR Damper

To design the MR damper model, the mathematical design suggested by Spencer et al [27] is embraced in this research. The Figure 2 shows the corresponding mathematical expressions**.** The damping force of this model is expressed by Equation 11.

$$F = C_1 \dot{y} + K_1 (x - x_0) \quad (10)$$
$$C_1 \dot{y} = \alpha z + K_0 (x - y) + C_0 (\dot{x} - \dot{y}) \quad (11)$$
$$\dot{z} = -\gamma |\dot{x} - \dot{y}| z |z|^{n-1} - \beta (\dot{x} - \dot{y}) |z|^n + A(\dot{x} - \dot{y}) \quad (12)$$
$$\alpha(I) = \alpha_a + \alpha_b (I) \quad (13)$$
$$C_1 = C_1(I) = c_{1a} + c_{1b} I \quad (14)$$
$$C_0 = C_0 I = c_{01a} + c_{o1b} I \quad (15)$$

where x is the comparative displacement across the damper, x and y are two transformative variables. Parameter$k_0, k_1, c_{0a}, c_{0b}, c_{1a}, c_{1b}, x_0, \gamma, \mu, A, n, \alpha_a$ and α_b are utilized to portray the MR damper.

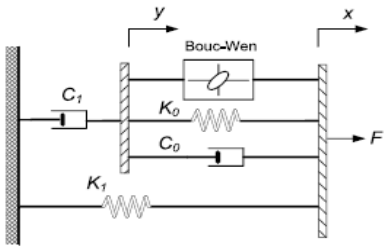

Figure 2: Mechanical model of the MR damper

4. Finite Element Analysis and Characterization

EMS is a 3D electromagnetic field simulator software suite that brides electrical and mechanical phenomena, based on the powerful finite element method and it is Add-in to SolidWorks. EMS has Electrostatic, Magneto static, AC-Magnetic, Transient Magnetic and motion analysis modules. All materials are applied from EMS materials browser. After setting the material properties, temperature and forces are applied to the model from the menu. For calculating the upstroke and down stroke force delivered by the damper, the moving body of the damper's model and its direction is selected. The next step is meshing which is an important part of the computer aided engineering simulation and finite element simulation process. Figure 3 represents the meshed image of the energy generated by MR damper's 3D model.

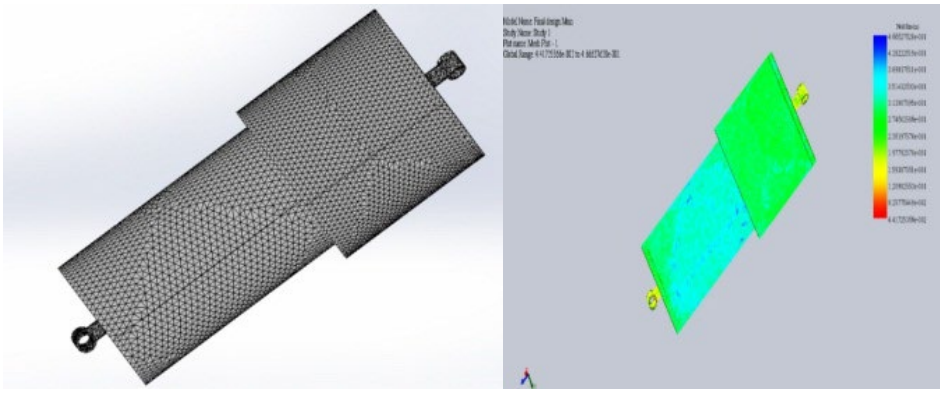

(a) (b)

Figure 3 (a) Meshing of the MR damper Model, (b) Finite element mesh plotting of the MR damper model

The geometry of the mesh is triangular and global mesh size is 4.5 mm and tolerance is 0.04%. The mesh plotted image of the model is exposed in Figure 3 (b), which is accomplished by using mesh plot tools of EMS. From Figure

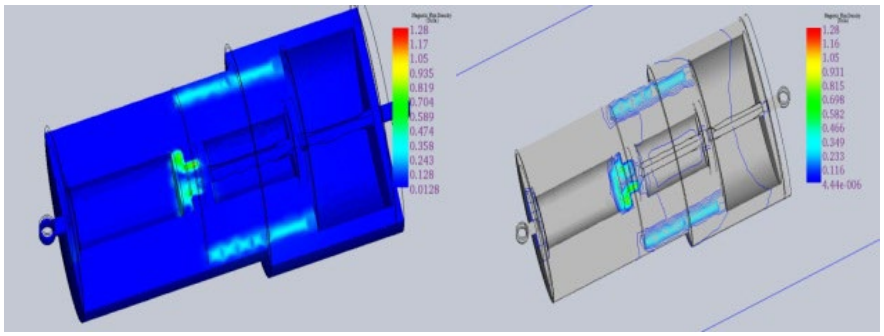

(a) (b)

Figure 4: Cross section clipping view of magnetic flux density (a) Continues fringe view and (b) Line fringe view

3 (b) it is observed that the global range of mesh size varies from 4.66 mm to 4.41 mm which depends on material properties as mesh size is assumed different for different materials. For characterizing energy generated MR damper magnetic flux density, magnetic field intensity, current density, temperature gradient and heat flux density has examined briefly for different input excitation current by EMS finite element analysis. Firstly magnetic flux density is considered for different excitation current varies from 0.1 A to 1.2 A. Figure 4 (a) and (b) represents the cross section clipping view, contour plotting of fringe view and Figure 5 presents the vector plotting of magnetic flux density of energy generated MR damper.

In Figure 4 (a), actually the magnetic flux density value is represented in tesla for an excitation current of 1 A where the flux density varies from 0 to 1.28 Tesla in the damper body. Observing closely is obvious that higher flux density is produced around the inside piston coil area and the permanent magnet area which is expressed by the color variation. For more clear inspection of the magnetic flux density distribution, the vector plot results are observed by ignoring X, Y and Z axis respectively which is illustrated in Figure 5.

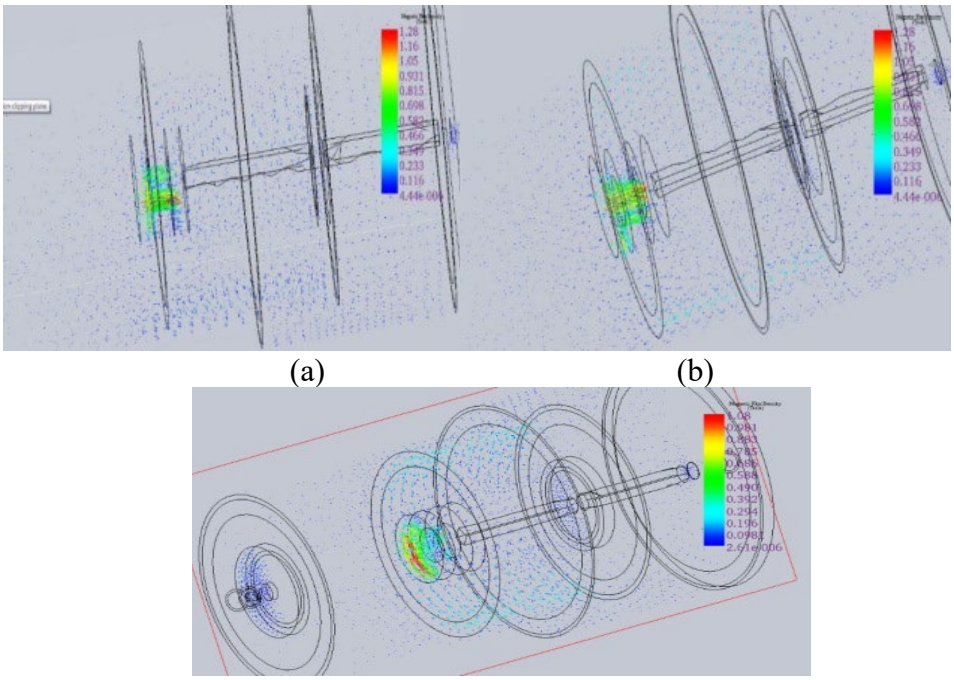

Figure 5 (a)(b)(c). Magnetic flux density of energy saving MR damper (X, Y and Z vector plotting)

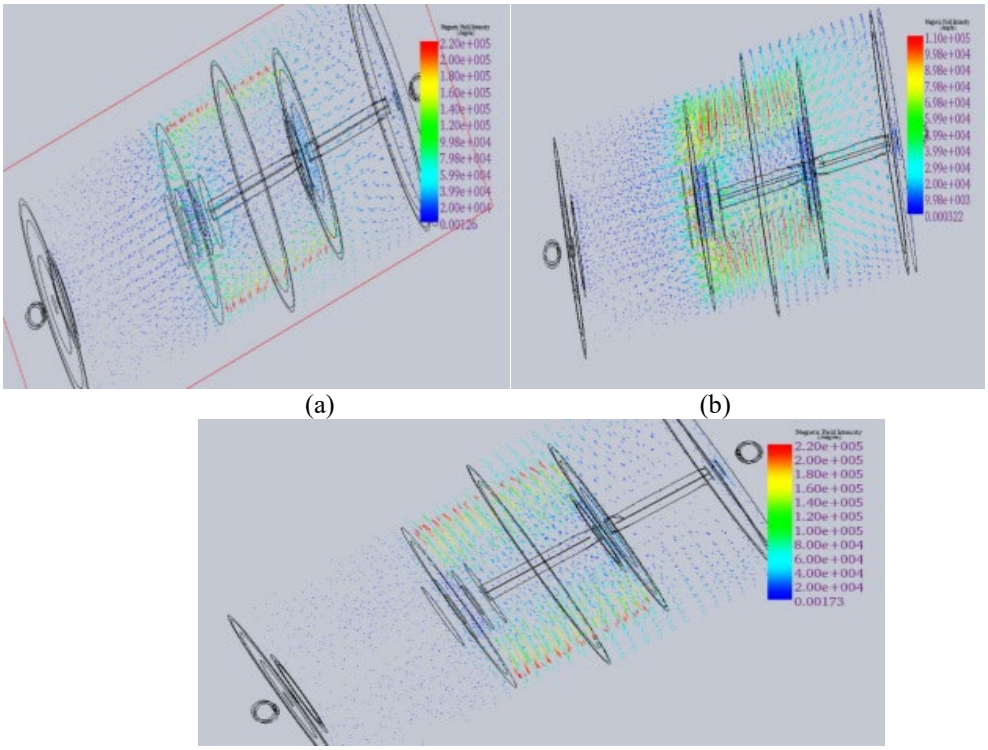

Figure 6: Magnetic field intensity of model (X, Y and Z vector plotting)

By examining Figure 5 it is observed that when any of the axis is ignored the magnetic flux density has reduced by small amount compare to Figure 4 (a) and (b). Another observation is the direction of the magnetic flux vector, which is not similar to ignoring the different axis and magnetic flux density inside the piston coil is higher than the permanent magnet. Figure 6 represents the magnetic field intensity of the energy saving MR damper model which actually expresses the intensity of magnetic field around the permanent magnet and piston coils due to the supplied current to excitation coils.

It is seen from the Figure 7 (a) that magnetic field spread inside the outer coil. The outer coil is moving along with piston rod, so these moving coils are facing the induced magnetic flux as presented above. According to Faraday's law a voltage is induced in those outer coils. These outer coils are connected to the inner coils. These inner coils are being used as a load to the outer coils. This close path creates opportunity to outer coils for supplying current to the inner coils where the amount of current depends upon the frequency of the piston rod movement. Figure 7 (b) is a representation of the cross-section line view of the magnetic field intensity distribution in the damper's body. The

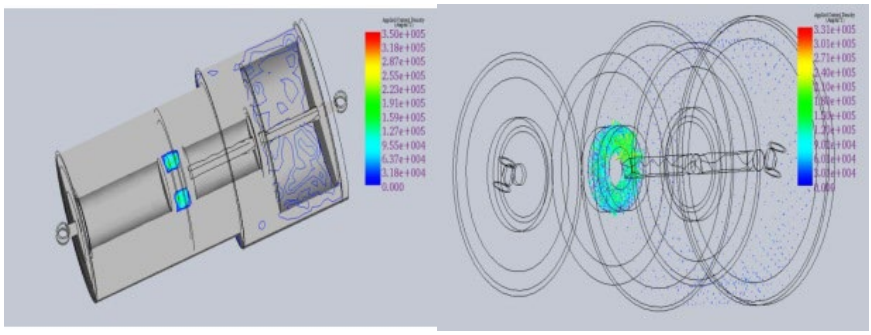

Figure 7: Applied current density of the model (a) Fringe line and (b) Vectot plotting view

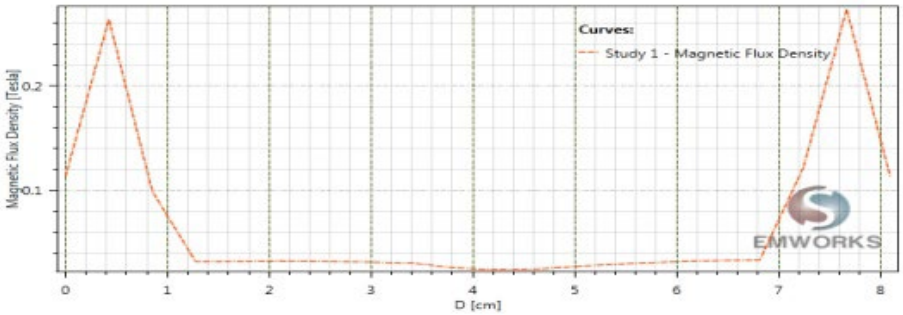

Figure 8: Magnetic flux density variation with respect to distance (permanent magnet's diameter)

magnetic field intensity has higher value around permanent magnet and MR fluid gap area as it is expected to control the damping force more accurately. For understanding the magnetic field intensity produced by the coils is analyzed by finite element vector plotting by ignoring the X, Y and Z axis correspondingly as exposed in Figure 8.
For understanding the magnetic field intensity produced by the permanent magnet and the coils, it is analyzed by finite element vector plotting by ignoring the X, Y and Z axis correspondingly as exposed in Figure 8. The magnetic field intensity is not same among the three Figures, such as the magnetic field intensity is different at the three different axis. The direction of the intensity vectors is altered in those images. Figure 8 is a representation of cross-sectional fringe line view of the piston heads applied current density.

One important feature of this damper from Figure 8 is that the applied current density has higher value in the piston coil area and little current is produced inside the damper's outer coil. From the vector plotting generally two things are observable and they are the direction and intensity of the applied current at each point of the coil.

5. Simulation Result and Discussion

Energy generated MR damper's finite element model has been built in EMS for characterization. EMS simulation establishes values at every global mesh node of the model. So here in the finite element analysis of the energy generated MR damper, nodal solution results are used for characterizing the damper's design where the excitation current was maintained at 1 A. At first 2D magnetic flux density results from EMS have analyzed. The 2D model's magnetic flux density plot from the simulation results is shown in Figure 9.

Figure 9 shows relation between the magnetic flux density and the distance. The distance is the permanent magnet's diameter, which is considered at a certain level above the piston head situated inside the damper cylinder wall. Figure 9 showed that the magnetic flux density increases at a closer distance to the permanent magnet. The event of going away from the permanent magnet magnetic flux density decreases rapidly as they are approaching to the non-magnetic materials zone. This magnetic flux density is almost zero inside non-magnetic materials situated between the two walls of the damper, the MR fluid inside the damper is not affected by the flux of the outside permanent magnet. So, there is no magnetic field interaction between the inner and outer magnetic field. The great achievement of this work

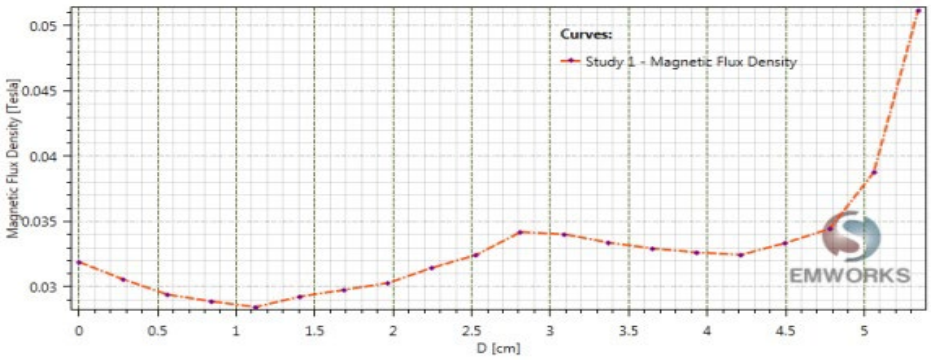

Figure 9: Magnetic flux density VS distance between two non-magnetic walls (through piston head)

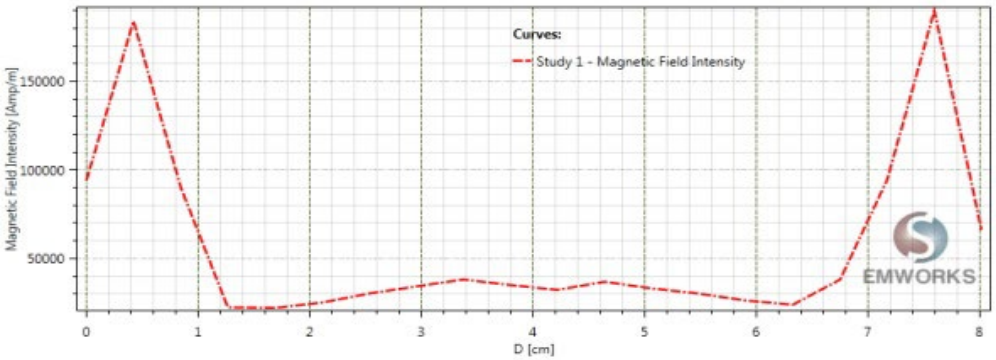

Figure 10 : Magnetic field intensity variation with respect to distance (permanent magnet's diameter)

is due to the successful magnetic field isolation between closely situated two magnetic sources. This magnetic isolation is accomplished by using nonmagnetic materials solid plastic. After the non-magnetic material wall, the magnetic flux density again increases dramatically in the other side's permanent magnet wall which is illustrated in the last part of the Figure 9. Figure 10 expresses the variation of magnetic flux density for a distance between two non-magnetic walls, here the distance is considered through the piston head.

Figure 11 it is seen that the magnetic flux density is slightly decreasing as it is going away from the permanent magnet area and it becomes almost zero just after the non-magnetic isolation. Then a slight increment is observed up to near about 3 cm which is the area from the non-magnetic isolation to piston head coil. After that a slow decrement of the flux is noticed up to 4.2 cm i.e. the other side non-magnetic wall. Again, the sharp rise of the magnetic flux density is noted in the last portion of the graph which is the high flux density in the other permanent magnet wall. Figure 11 the magnetic field intensity variation model through permanent magnet generator's diameter, which is also considered at a certain level above the piston head situated inside the damper cylinder wall.The initial and ending higher magnetic

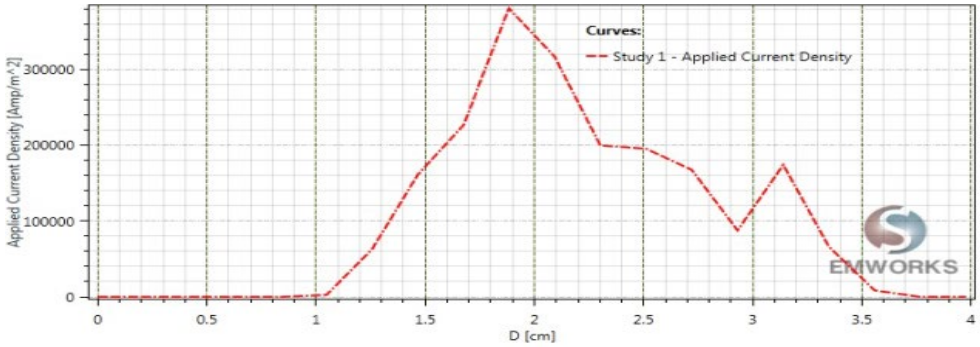

Figure 11: Applied current density variation in distance between two non-magnetic walls (through piston head)

field intensity in the graph represents two permanent end walls higher value. In the middle region, there is a small rise of intensity due to the induced magnetic field in nearer piston head coils.
Figure 12 articulates the variation of applied density for a distance between two non-magnetic walls where the distance is considered through the piston head.

It can be said from Figure 12, inside the damper wall and MR fluid gap there is no applied current density, which is presented in 0 to 1 cm distance in the above graph. But this applied current density increases sharply from the damper wall region to the piston coil inner side as the current is applied in the coils. After that, applied current density decreases gradually from the piston coil to the damper wall. Figure 12 presents the applied current density variation of the damper model through outer coil wall's diameter.

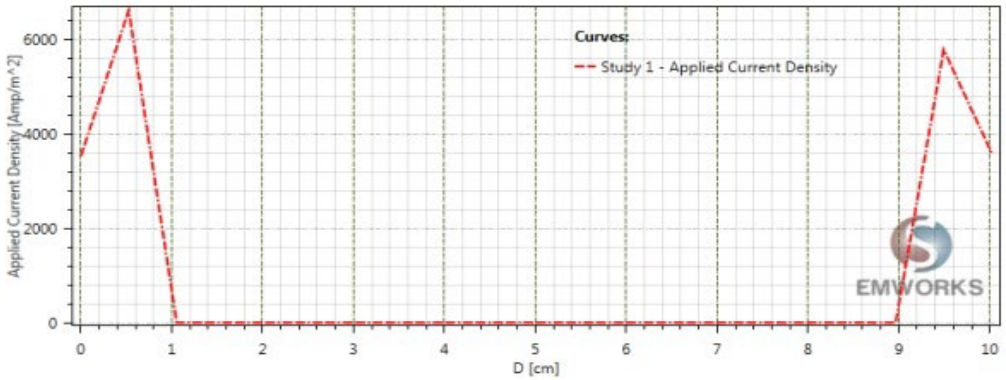

Figure 12: Variation of applied current density through outer coil diameter

From Figure 12 it's obvious that the current is produced inside the outer coil of the model which is represented by the higher value of the applied current density of the starting and the end of the above graph value of applied current density is almost zero between the two opposite walls of the outer coil. So, overall results its observed that the permanent magnet in the outer body generates magnetic flux. When it is moving along with piston rod these fluxes are cut by outer body coils. As cut by changing flux energy induced in these coils which works as a power supply to the inner coil. These supplying currents from the outer coil to the inner coil depend upon the relative motion between the permanent magnet and outer coil. It can be concluded from this advanced finite element analysis that the proposed model is successfully working as self-powered and energy saving MR damper.

6. Conclusion

Advancement in MR damper technology is one of the challenging researches in the vibration control area. In this study a mono tube MR damper model is developed which has power generation competence. Here solid works EMS based finite element analysis is accomplished for characterizing and validating the model's accuracy of power generation. In this damper model permanent magnets and coils are used as power generators that utilize wasted vibration energy from the environment. In this energy generated damper's EMS analysis MR fluid gap width, outside air gap width, gap length, permanent magnet length, permanent magnet thickness, non-magnetic material thickness, piston head, coil housing thickness, diameter of the piston head, the number of coil turns, different materials used in overall model are selected as design parameters for model's accuracy. From EMS electromagnetic analysis magnetic flux density, magnetic field intensity, temperature, the applied current density has been examined to characterize the power generation feature and all the results are clearly validating that quality. The magnetic isolation between the two separated fields has been observed clearly from those results. So, it can be concluded that the developed mono tube MR damper model works effectively as an energy generated device.

References

Kordonsky, W.: Elements and Devices Based on Magnetorheological Effect*. Journal of Intelligent Material Systems and Structures 4(1), 65-69, 1993.

Graff, P., Feroz, F., Hobson, M. P., & Lasenby, A., Neural Networks for Astronomical Data Analysis and Bayesian Inference. 2013 IEEE 13th International Conference on Data Mining Workshops, 16–23, 2013.

Lai, C.Y., Liao, W.-H.: Vibration control of a suspension system via a magnetorheological fluid damper. Journal of Vibration and Control **8**(4), 527-547, 2002.

Greenwood, A. J. B., Schoups, G., Campbell, E. P., & Lane, P. N. J. , Bayesian scrutiny of simple rainfall – runoff models used in forest water management. JOURNAL OF HYDROLOGY, 512, 344–365, 2014.

Nikam, V. B., & Meshram, B. B., Modeling Rainfall Prediction Using Data Mining Method: A Bayesian Approach. 2013 Fifth International Conference on Computational Intelligence, Modelling and Simulation, 132–136, 2013.

Shakil S M., and Ullah M. S., "Analyzing the Operational Parameters of a Single Walled Carbon Nanotube Field Effect Transistor (SWCNT-FET)," Proceedings of the 8th North American International Conference on Industrial Engineering and Operations Management (IEOM 2023), Houston, Texas, USA, 13 -15 June 2023.

Shakil S M., and Ullah M. S., "Reliability Issues in Current MOSFET and Beyond Silicon Technology," Proceedings of the 8th North American International Conference on Industrial Engineering and Operations Management (IEOM 2023), Houston, Texas, USA, 13 -15 June 2023.

Greenwood, A. J. B., Schoups, G., Campbell, E. P., & Lane, P. N. J. (2014). Bayesian scrutiny of simple rainfall – runoff models used in forest water management. JOURNAL OF HYDROLOGY, 512, 344–365, 2014.

Liu, Y., Automatic calibration of a rainfall-runoff model using a fast and elitist multi-objective particle swarm algorithm. Expert Systems with Applications, 2009.

Rashid, M. M., Romlay, M. R. M., & Ferdaus, M. M., Development of Electronic Rain Gauge System. International Journal of Electronics and Electrical Engineering, 3(4), 245–249, 2015.

Shabir A., and Ullah M., "Heat transfer characteristics of CNT with chirality engineering for solar cell application," *In 2022 IEEE International Semiconductor Conference (CAS 2022),* Barsov, Romania, 12-14. October 2022, pp. 159 -162.

Shakil S.M. and M. S. Ullah. "Effects of NBTI On PMOS Device With Technology Scaling." *2022 IEEE 13th Annual Ubiquitous Computing, Electronics & Mobile Communication Conference (UEMCON 2022)*, NY, USA, 26 - 29 October 2022, pp. 0402 - 0406.

Shabir A., and Ullah M., (2022) "Investigation of the emerging materials based high-efficiency cdte solar cell," *Proceedings of the 7th North American International Conference on Industrial Engineering and Operations Management (IEOM 2022)*, Orlando, USA, 11 -14 June 2022, pp. 2698-2706.

Amin A.B., S. M. Shakil and M. S. Ullah, "A Theoretical Modeling of Adaptive Mixed CNT Bundles for High-Speed VLSI Interconnect Design," *Crystals*, vol. 12, no. 2, pp. 186-201, January 2022.

Shabir A., and Ullah M., (2022)"Chirality Engineering on CNTs - A New Approach to Boost the Solar Cell Efficiency," *Proceedings of the 7th North American International Conference on Industrial Engineering and Operations Management (IEOM 2022)*, Orlando, USA, 11 -14 June 2022, pp. 1705-1706.

Shabir, A., Cao, J., Fouad, E., & Ullah, M. W. (2022),"Prospects of solar cell technology from silicon to carbon nanotube," *In 2022 IEEE 9th International Conference on Sciences of Electronics, Technologies of Information and Telecommunications (SETIT 2022)*, Genoa, Italy, 19 -21 March 2022, pp. 385-391.

S. M. Shakil and M. H. Rashid, " The Potential Impacts of Wireless Power Transfer on the Global Economy, Society, and Environment," in *IEEE 14th Power Electronics, Drive Systems, and Technology Conference (PEDSTC)* 31 january – 02 Feb. 2023.

Shabir A., Zaidi B., Ullah M., (2023)"Carrier Generation Ability of CNTs to Harvest Maximum Energy from Solar Spectrum, "*IEEE SoutheastCon 2023"*, Orlando, USA, 14-16 April 2023, pp. 399-404.

S M Shakil, Muhammad Sana Ullah, "Analysis of HCD Effects for NMOS Transistor with Technology Scaling", *SoutheastCon 2023*, pp.445-449, 2023.

Shabir, A., & Ullah, M., "Explore the chirality engineering of carbon nanotubes for solar cell". *Florida Scientist, vol.85, no.*2,pp. 68, 2022.

Report: IEA-PVPS T13-02:2014, Characterization of performance of thin-film Photovoltaic Technologies, PVPS-Photovoltaic Power Systems Programme, IEA-International Energy Agency, May 2014.

Sites J. and Pan J., "Strategies to increase CdTe solar-cell voltage," "*Thin Solid Films"*, vol. 515, no. 15, pp. 6099–6102, 2007.

Debnath Atanu., Uddin MN., et al "Underwater Surveillance Autonomous Boat," Proceedings of the 8th North American International Conference on Industrial Engineering and Operations Management (IEOM 2023), Houston, Texas, USA, 13 -15 June 2023.

Debnath Atanu., Uddin MN., et al "Current Scenario of Solar Home Systems and Future Utilization in Bangladesh," Proceedings of the 8th North American International Conference on Industrial Engineering and Operations Management (IEOM 2023), Houston, Texas, USA, 13 -15 June 2023.

Tursun A. and Joel N., "Thin-Film Solar Cells with 19% Efficiency by Thermal Evaporation of CdSe and CdTe". "*ACS Energy Letters",* vol, *5 no.*3, pp. 892-896, 2020.

Ullah H., Marí B., Cui H., "Investigation on the effect of Gallium on the efficiency of CIGS solar cells through dedicated software*", Applied Mechanics and Materials*, Vol. 448, pp. 1497- 150, 2014.

Wu X., Keane J., et al, "16.5%-efficient CdS/CdTe polycrystalline thin-film solar cell," in *Proc. 17th Eur. Photovoltaic Sol. Energy Conf*., , pp. 995–1000. 2001.

Zaidi, B., Shekhar C., K. Kamli, Z. Hadef, S. Belghit, and Ullah S,. "Junction Configuration Effect on the Performance of In2S3/CZTS Solar Cells." *Sumy State University,* 2020.

Zaidi, B., M. S. Ullah, S. Zahra, S. Gagui, and C. Shekhar. "Analysis of I-V-T Characteristics of CH3NH3PbBr3 Perovskite Based Solar Cells." *Journal of Nano- & Electronic Physics* . Vol. 13 Issue 5, p05016-1-05016-4. 4p, 2021.

Madiha M. “The development of neural network based rainfall-runoff model for Kashmir Pakistan” *8th North American Conference on industrial Engineering and Operational Management* ; Houston Taxas, USA . June 13-15. 2023.

Madiha M. “Present and Future Commercial Applications of Carbon Nanotubes: A Review ” *8th North American Conference on industrial Engineering and Operational Management* ; Houston Taxas, USA . June 13-15. 2023.

Zaidi, B., Ullah M., et al" Role of TCO Films in Improving the Efficiency of CdS/MoS2 Heterojunction Solar Cells." *Journal of nano-and electronic physics,* vol.11, no. 2, pp. 02030-1, 2019